Rational Design of a Transition State Analogue with Picomolar Affinity for Pseudomonas aeruginosa PvdQ, a Siderophore Biosynthetic Enzyme

ARTICLE *in* ACS CHEMICAL BIOLOGY · JULY 2013

Impact Factor: 5.33 · DOI: 10.1021/cb400345h · Source: PubMed

5 AUTHORS, INCLUDING:

Dali Liu
Loyola University Chicago
32 PUBLICATIONS **434** CITATIONS

ACS chemical biology

Articles

pubs.acs.org/acschemicalbiology

Rational Design of a Transition State Analogue with Picomolar Affinity for *Pseudomonas aeruginosa* PvdQ, a Siderophore Biosynthetic Enzyme

Kenneth D. Clevenger,[†] Rui Wu,[¶] Joyce A. V. Er,[‡] Dali Liu,*[,¶] and Walter Fast*[,‡]

[†]Department of Chemistry and Biochemistry and the [‡]College of Pharmacy, Medicinal Chemistry Division, University of Texas, Austin, Texas 78712, United States

[¶]Department of Chemistry and Biochemistry, Loyola University Chicago, Chicago Illinois 60660, United States

Supporting Information

ABSTRACT: The *Pseudomonas aeruginosa* enzyme PvdQ can process different substrates involved in quorum-sensing or in siderophore biosynthesis. Substrate selectivity was evaluated using steady-state kinetic constants for hydrolysis of *N*-acyl-homoserine lactones (HSLs) and *p*-nitrophenyl fatty acid esters. PvdQ prefers substrates with alkyl chains between 12 and 14 carbons long that do not bear a 3-oxo substitution and is revealed here to have a relatively high specificity constant for selected *N*-acyl-HSLs (k_{cat}/K_M = 10^5 to 10^6 M^{-1} s^{-1}). However, endogenous *P. aeruginosa* *N*-acyl-HSLs are ≥100-fold disfavored, supporting the conclusion that PvdQ was not primarily evolved to regulate endogenous quorum-sensing. PvdQ plays an essential biosynthetic role for the siderophore pyoverdine, on which *P. aeruginosa* depends for growth in iron-limited environments. A series of alkylboronate inhibitors was found to be reversible, competitive, and extremely potent (K_i ≥ 190 pM). A 1.8 Å X-ray structure shows that 1-tridecylboronic acid forms a monocovalent bond with the *N*-terminal *β*-chain Ser residue in the PvdQ heterodimer, mimicking a reaction transition state. This boronic acid inhibits growth of *P. aeruginosa* in iron-limited media, reproducing the phenotype of a genetic *pvdQ* disruption, although co-administration of an efflux pump inhibitor is required to maintain growth inhibition. These findings support the strategy of designing boron-based inhibitors of siderophore biosynthetic enzymes to control *P. aeruginosa* infections.

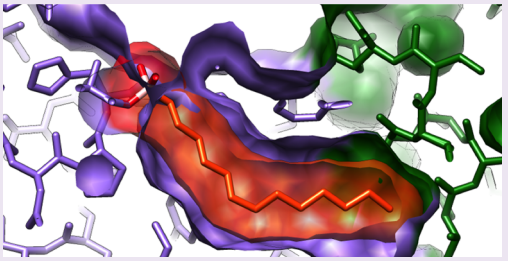

The human opportunistic pathogen *Pseudomonas aeruginosa* is a worldwide clinical threat associated with diverse nosocomial infections that are increasingly difficult to treat.[1] To develop novel therapeutics, new antimicrobial targets have been proposed, including pathways that facilitate iron acquisition and those that regulate quorum-sensing.[2,3] The protein PvdQ is an unusual example found at the nexus of these two pathways because its enzymatic function has been proposed to play roles both in siderophore production and in degradation of some *N*-acyl-homoserine lactone (HSL) signaling molecules.[4,5]

P. aeruginosa requires iron (Fe^{3+}), which is only sparingly soluble and is found at a concentration of 10^{-24} M in serum in its free form.[6] In response, biosynthetic pathways have evolved to produce two siderophores, pyoverdine and pyochelin, that are released into the surrounding environment to scavenge iron and to shuttle it back, with pyoverdine being the predominant iron supplier.[7] Siderophore biosynthetic enzymes have been suggested as novel antibiotic targets since inhibitors would block iron acquisition and severely limit bacterial growth in host tissues. This strategy has been shown to be effective with *Mycobacterium tuberculosis*, *Yersinia pestis*, and recently, *P. aeruginosa*.[8−11] As illustration of this concept, a genetic knockout of *P. aeruginosa* *pvdQ*, which encodes a key enzyme in pyoverdine biosynthesis, results in a bacterial strain that does not produce pyoverdine, is growth inhibited in an iron-limited medium, and has reduced virulence in plant and animal models of infection.[12] A small molecule inhibitor of PvdQ can also inhibit growth in a iron-limited medium.[11]

A second notable feature of PvdQ is its ability to function as a quorum-quenching enzyme. Artificial constitutive expression of PvdQ (which is typically only upregulated during iron starvation) or addition of exogenous purified PvdQ prevents accumulation of the quorum-sensing signal *N*-3-oxo-doecanoyl-HSL (3-oxo-C12-HSL) and reduces production of the virulence factors pyocyanin and elastase.[4,13] It has been suggested that the primary biological function of PvdQ is siderophore biosynthesis and not regulation of quorum-sensing.[5,12] Nevertheless, its ability to degrade *N*-acyl-HSLs can still be a useful activity. For example, administration of PvdQ as a therapeutic enzyme has been proposed to limit quorum-sensing-dependent virulence in pulmonary *P. aeruginosa* infections.[14]

Regardless of whether one's goal is to develop an inhibitor to block PvdQ action in iron acquisition or to develop a quorum-quenching enzyme, understanding how PvdQ recognizes and

Received: May 15, 2013
Accepted: July 24, 2013
Published: July 24, 2013

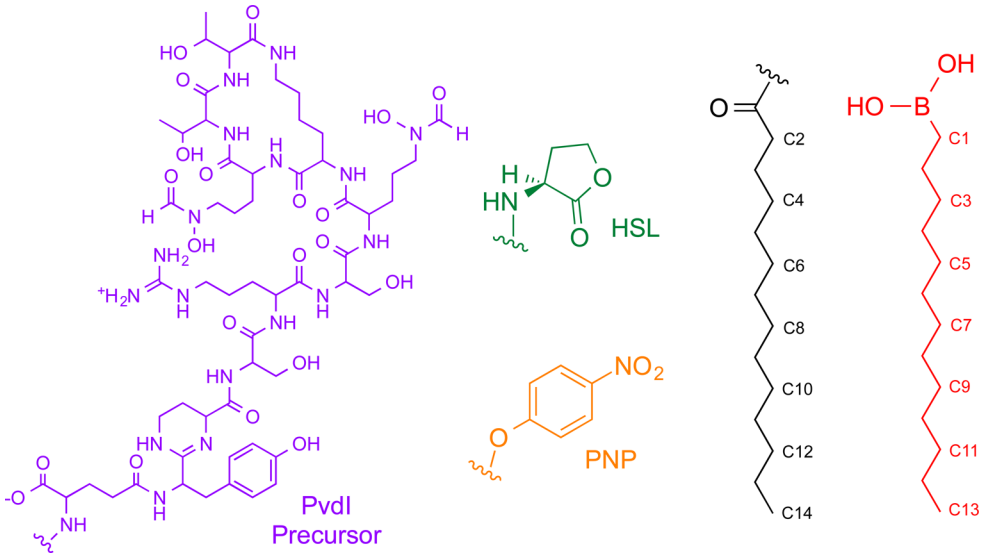

Figure 1. Selected PvdQ Ligands. The C14 alkyl substitution (black) of a PvdI precursor (purple) is removed by PvdQ-catalyzed amide hydrolysis. The *N*-acyl substitutions of varying length (black) on *N*-acyl-L-homoserine lactones (HSL, green) are hydrolyzed by PvdQ, as are the corresponding *p*-nitrophenol (PNP, orange) esters. *N*-Acyl-HSLs with 3-oxo substitutions bear a carbonyl at C3 (not pictured). Alkylboronic acids (C_n-$B(OH)_2$, red) are inhibitors of PvdQ.

processes ligands provides information valuable for improving the desired outcome. Herein, we quantify substrate selectivity and use this information to rationally design a potent transition state analogue inhibitor of PvdQ that is applied in structural and cell-based studies. The implications of these findings for understanding the catalytic mechanism, for designing more effective inhibitors as molecular probes or therapeutics, and for developing more effective quorum-quenching enzymes are discussed.

RESULTS AND DISCUSSION

Substrate Selectivity. To quantify the selectivity of PvdQ for different *N*-acyl-substrates, we determined steady-state kinetic parameters for a series of substrates (Figure 1, Table 1). C12-HSL is a good substrate (k_{cat}/K_M = 10^5 M^{-1} s^{-1}), but shorter acyl chains are only very poorly hydrolyzed ($k_{cat}/K_M \leq 10^3$ M^{-1} s^{-1}) (Figure 1, Table 1). Notably, 3-oxo-C12-HSL is a poor substrate. Therefore, PvdQ does not appear to be optimized for hydrolysis of either C4-HSL[13] or 3-oxo-C12-HSL, the two endogenously produced *N*-acyl-HSLs of *P. aeruginosa*. These results are consistent with qualitative studies showing a preference for substrates with acyl chains of at least 8 carbons.[4] Although these results suggest that PvdQ was not evolutionarily optimized to regulate endogenous *P. aeruginosa* signaling, this activity of PvdQ is still useful as a biochemical tool for degrading certain *N*-acyl-HSLs. For example, the specificity constants of PvdQ for selected substrates compares favorably with quorum-quenching enzymes from different superfamilies such as AiiA from *Bacillus thuringiensis* (dizinc metalloform k_{cat}/K_M values ≈ 10^4 M^{-1} s^{-1}; dicobalt metalloform k_{cat}/K_M ≈ 10^6 M^{-1} s^{-1}),[15] and an engineered version of PLL from *Mycobacterium avium* (k_{cat}/K_M ≈ 10^4 M^{-1} s^{-1}), indicating that PvdQ might serve equally well to degrade certain *N*-acyl-HSLs.[16]

Table 1. Steady-State Rate Constants for PvdQ-Catalyzed Hydrolysis of Selected Substrates

substrate	K_M (μM)	k_{cat} (min^{-1})	k_{cat}/K_M (M^{-1} s^{-1})
C8-HSL	ND[a]	ND	2.2 × 10^2 [b]
C10-HSL	ND	ND	2.2 × 10^3 [b]
C12-HSL	11 ± 2	148 ± 7	2.2 × 10^5
3-oxo-C12-HSL	ND	ND	2.3 × 10^3 [b]
C10-PNP	61 ± 13	49 ± 5	1.3 × 10^4
C12-PNP	0.8 ± 0.1	52 ± 3	1.1 × 10^6
C14-PNP	0.60 ± 0.06	86 ± 3	2.4 × 10^6
C16-PNP	4 ± 1	1.9 ± 0.1	8 × 10^3

[a]ND: not determined because limited substrate solubility prevents determination of V_{max}. [b]Fitting error is ≤8%.

Unlike these other quorum-quenching enzymes,[15,17] PvdQ appears to tolerate different ring substitutions yet is more selective for chain length. So, we defined the selectivity of PvdQ more precisely by comparing steady-state kinetic constants for *p*-nitrophenyl fatty acid ester reporter substrates (Figure 1, Table 1). Notably, the k_{cat}/K_M values measured here are signifignatly larger than earlier reports[18] due mostly to lower K_M values, possibly reflecting increased substrate solubility in our assay conditions (see Methods). PvdQ preferentially hydrolyses substrates with 12−14 carbon alkyl chains, with shorter or longer chains showing ≥2 orders of magnitude decrease in k_{cat}/K_M (Table 1). Taken together, these findings suggest that PvdQ has evolved in response to a need for processing myristoylated substrates and has not been optimized for the endogenous quorum-sensing signals of *P. aeruginosa* (although moonlighting[19] roles are possible). This conclusion is consistent with the proposed primary role of PvdQ in processing myristoylated precursors of the siderophore pyoverdine (Figure 1).[5,12]

Inhibitor Design. Two previous reports of high-throughput screening for PvdQ inhibitors describe the discovery of structurally diverse inhibitors. Two compounds of moderate potency, NS2028 (8-bromo-4*H*-[1,2,4]oxadiazolo[3,4-*c*][1,4]-benzoxazin-1-one; IC_{50} = 130 μM) and SMER28 (6-bromo-*N*-(prop-2-en-1-yl)quinazolin-4-amine; IC_{50} = 65 μM) were identified from a 1280-compound library of bioactive compounds (LOPAC) and determined by X-ray crystallography to bind in the myristoyl binding pocket, predominantly

dx.doi.org/10.1021/cb400345h | ACS Chem. Biol. 2013, 8, 2192−2200

through hydrophobic interactions.[18] A more potent inhibitor, ML218 (2-(4-fluorophenyl)-2-(6-(trifluoromethyl)pyridine-2-yl)acetonitrile; IC_{50} = 6 nM) was recently discovered by screening the NIH molecular libraries probe production centers network compound library.[11] The mode of inhibition for ML218 was not reported, but micromolar concentrations were shown to inhibit growth of *P. aeruginosa* in an iron-limited medium.

Taking an alternative rational design approach, we first started with a boronate moiety since these are known inhibitors of other Ser/Thr-dependent hydrolases[20,21] and then proposed a series of alkyl substitutions that mimic the observed substrate preference. Potency varies with chain length, with C12- and C13-$B(OH)_2$ having the lowest K_i values (~200 pM) (Table 2). Please note that the C13-$B(OH)_2$ inhibitor is the closest structural match to myristoylated (C14) substrates because the boron takes the position of the initial carbon in the corresponding substrate (Figure 1). The mode of inhibition for C12- and C13-$B(OH)_2$ was determined to be competitive (Figure 2, Supplementary Figure 1). We did not observe any time-dependent onset of inhibition and some activity was restored upon dialysis (not shown) consistent with a rapid equilibrium reversible mode of inhibition. The boronic acid moiety is clearly important for potency since fatty acids are several orders of magnitude less potent (Table 2, Supplementary Figure S2). These inhibitors are at least 325,000-fold more potent than the two previously reported compounds known to bind at the alkyl-binding site.[18]

Table 2. K_i Values for Alkylboronic and Fatty Acid Inhibitors of PvdQ

inhibitor	K_i (nM)
C8-$B(OH)_2$	161 ± 3
C10-$B(OH)_2$	1.1 ± 0.4
C12-$B(OH)_2$	0.19 ± 0.02
C13-$B(OH)_2$	0.20 ± 0.04
C14-$B(OH)_2$	1.0 ± 0.3
C15-$B(OH)_2$	8.3 ± 0.9
C12-COOH	6000 ± 200

Due to the potency of the alkylboronic acid inhibitors and their ability to form reversible tetrahedral adducts, we suspected that they act as transition state mimics. In general, the free energy of binding transition state analogues is expected to parallel the free energy of transition state stabilization for a structurally similar series of substrates.[22] However, the structural offset of the inhibitors and substrates described here (Figure 1) precludes traditional linear comparison plots between the compounds tested. So instead, we sought to determine whether the $\Delta\Delta G_{bind}$ (calculated from K_i values) for changes in inhibitor chain length correlates with $\Delta\Delta G^{\ddagger}$ (calculated from k_{cat}/K_M values) for a similar series of substrates. When these $\Delta\Delta G$ values are plotted against normalized chain length (Figure 2), they clearly overlap, a result that is consistent with transition state mimicry. (Comparison of ΔG_{bind} for inhibitor with the free energy of ground state binding for substrate is not presented since the rate-limiting step for PNP ester substrates is not known and K_M may not be a useful substitute for K_d values.)

Structural Characterization. To test the proposed mode of inhibition, we determined a structure of the inhibited complex. In general, boron-containing inhibitors can bind noncovalently or bind through reversible mono-, di-, or tricovalent bonds with N or O nucleophiles.[21,23−26] Changes in inhibitor structure can even change which active-site residue is covalently modified.[27] These different possible binding mechanisms make *a priori* predictions problematic. So, we grew cocrystals of C13-$B(OH)_2$ inhibited PvdQ at pH 7.5 and determined the X-ray crystal structure at 1.8 Å resolution (Table 3, Figure 3, and Supplementary Figures S3 and S4). The structure of PvdQ in complex with C13-$B(OH)_2$ was solved in space group $C222_1$. The final model was built as a heterodimer and comprises an α subunit (residues 28−192) and a β subunit (residues 217−907) as a result of autoproteolysis. Ligand atoms were refined with occupancies of 1 and *B*-factors ranging from 18.45 to 44.97. The overall structure of the protein resembles a 'V'-shape (Supplementary Figure S3). The active site, including

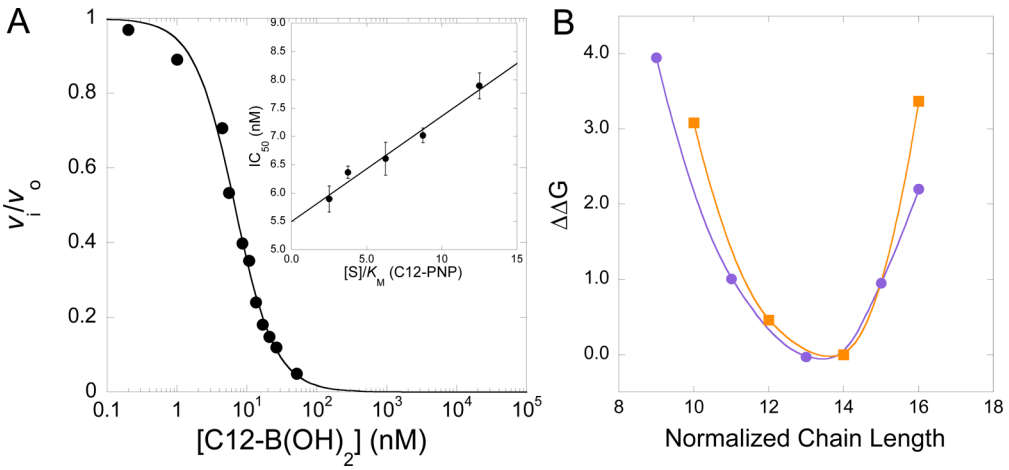

Figure 2. Competitive tight-binding inhibition of PvdQ by C12-$B(OH)_2$. (A) IC_{50} values were determined for the inhibitor using varying concentrations of C12-PNP substrate. Main panel shows a representative plot with 5 μM substrate. Inset shows a linear dependence of IC_{50} on [S]/K_M, indicating competitive inhibition. (B) Free energy correlation between K_i and k_{cat}/K_M for a structurally related set of inhibitors and substrates. Inhibitors are designated using their chain length +1 to account for boron at the initial position (Figure 1). The $\Delta\Delta G_{bind}$ for inhibitor K_i values (purple ●) relative to that of the normalized C14 length are plotted along with $\Delta\Delta G^{\ddagger}$ values for k_{cat}/K_M of PNP substrates (orange ■) relative to C14-PNP.

dx.doi.org/10.1021/cb400345h | *ACS Chem. Biol.* 2013, 8, 2192−2200

Table 3. Crystallographic Statistics for C13-B(OH)$_2$-Inhibited PvdQ

Data Processing	
space group	$C222_1$
cell dimensions	
α, β, γ (deg)	90.0; 90.0; 90.0
a, b, c (Å)	121.0; 166.4; 94.2
resolution (Å)	41.0−1.8
mosaicity (deg)	0.33
R_{merge}[a] (%)	0.124 (0.603)[b]
I/σ	9.6 (2.1)
completeness (%)	99.7 (100)
multiplicity	6.3 (6.3)
no. Reflections	488124
no. unique reflections	86070
Refinement	
R_{work}[c]/R_{free}[d] (%)	16.23/18.78
no. of atoms	
protein	6304
ligand	22
water	598
B-factors (Å^2)	
overall average	29.5
protein average	23.68
ligand *B*-factor range	18.45/44.97
RMSD[e]	
bond length (Å)	0.007
bond angle (deg)	1.126
Ramachandran statistics (%)	
most favored	96.07
allowed	3.37
outliers	0.56

[a]$R_{merge} = \Sigma|I_{obs} - I_{avg}|/\Sigma I_{avg}$ [b]The values for the highest resolution bind are in parentheses. [c]$R_{work} = \Sigma|F_{obs} - F_{calc}|/\Sigma F_{obs}$. [d]Five percent of the reflection data were selected at random as a test set, and only these data were used to calculate R_{free}. [e]RMSD, root-mean-square deviation.

the catalytic N-terminal residue of the β subunit, Ser217, resides in a deep cleft that is large enough to accommodate the proposed siderophore precursor as a substrate.

The overall protein structure of PvdQ matches those previously reported except for differences near the active site (Supplementary Figure S3).[18,28] Structural comparison with one previously solved structure (PDB ID: 2WYE)[28] shows a RMSD of 0.3 Å for all Cα atoms. A simulated annealing composite omit map to remove phase bias reveals extra electron density at the active site (Figure 3) that is well fit by a covalent Ser217−C13-B(OH)$_2$ adduct. The inhibitor alkyl chain binds in the myristoyl-binding pocket and a monocovalent bond is formed between the inhibitor boron and the side chain alcohol of Ser217 (the N-terminal residue of the heterodimer β-chain) (Figure 3 and Supplementary Figure S4). The tight packing of the alkyl chain into the myristoyl-binding site helps explain the observed substrate preference (Table 1) because substrates longer than C14 would be disfavored by steric occlusion. It is less clear how PvdQ disfavors substrates shorter than C12. The side chains of several residues, including Phe240, Thr285, Val286, Val403, and Pro238, are found in close proximity ($\leq$5 Å) to C2 of the inhibitor, which corresponds to the position bearing the disfavored 3-oxo-substitutent in *N*-acyl-HSL substrates. Therefore, these residues likely contribute to the substrate preference of PvdQ for *N*-acyl-HSLs bearing acyl chains unsubstituted at the 3-carbon position.

Formation of a dative covalent bond between Ser217 and the inhibitor (Figure 3 and Supplementary Figure S4) results in an adduct that mimics an anionic tetrahedral reaction transition state, consistent with the observed correlation between $\Delta\Delta G_{bind}$ and $\Delta\Delta G^{\ddagger}$ values (Figure 2) and the contribution of the boronic acid moiety to potency (Table 2, Supplementary Figure S2). Previously, PvdQ crystals at low pH have been used to trap a covalent ester reaction intermediate.[18,28] Here, the use of a transition state mimic allows a representative structure of a reaction step to be obtained at pH 7.5, avoiding any structural perturbations due to altered pH conditions that inhibit catalysis and provides additional insight into catalysis.

Mechanistic Implications. The structure of a transition state analogue helps elucidate the catalytic mechanism. Previously, a mechanism has been proposed based on structures of the resting enzyme, a product complex, and a covalent ester intermediate trapped at low pH (Figure 4, paths 1b, 3b, 5b).[28] Here, we propose amendments resulting in a simplified mechanism that does not include product-assisted catalysis (Figure 4, paths 1a, 3a, 5a): Based on precedence in other superfamily members, a direct deprotonation of the Ser217 side chain by the *N*-terminal amine (path 1a), proceeds to attack of the bound substrate and formation of the first tetrahedral adduct.[29] The *N*-terminus may have a depressed pK_a due to nearby electropositive side chains of His239 (2.9 Å)

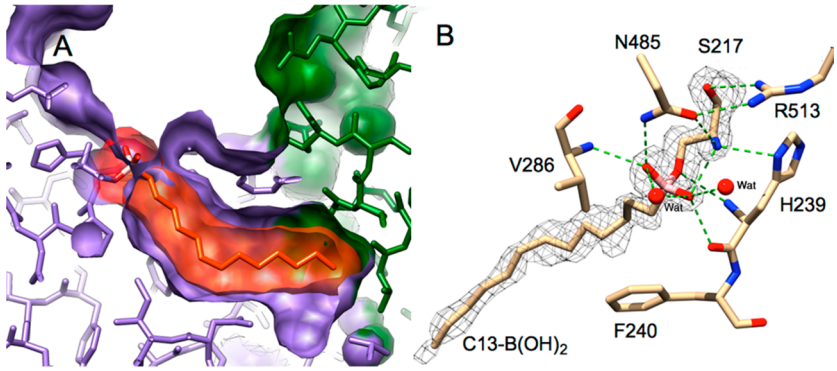

Figure 3. A 1.8 Å structure of PvdQ inhibited by C13-B(OH)$_2$. (A) Cutaway surface view showing the alkyl chain of the inhibitor (orange) bound to the myristyl-binding site of PvdQ, with the α subunit in green and the β subunit in purple. See Supplementary Figure S3 for a wider perspective. (B) A simulated annealing composite omit map at 1.1 σ showing a monocovalent adduct between the inhibitor's boron (pink) and the side chain of Ser217 (the *N*-terminal residue of the β-chain), with H-bonds and water molecules included.

dx.doi.org/10.1021/cb400345h | *ACS Chem. Biol.* 2013, 8, 2192−2200

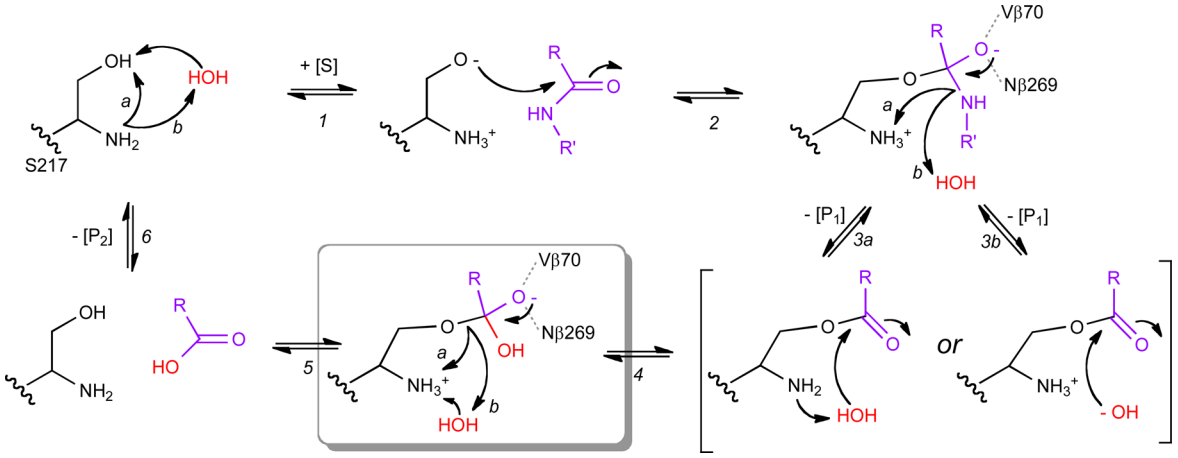

Figure 4. Proposed chemical mechanism for PvdQ. The C13-B$(OH)_2$–PvdQ complex most closely mimics the second tetrahedral intermediate (boxed). R′ is the PvdI precursor or HSL (Figure 1), which is released as an amine as the first product (P_1). R is an acyl chain that is released as a fatty acid as the second product (P_2). Results presented here favor the more parsimonious mechanism (paths a; see Results and Discussion).

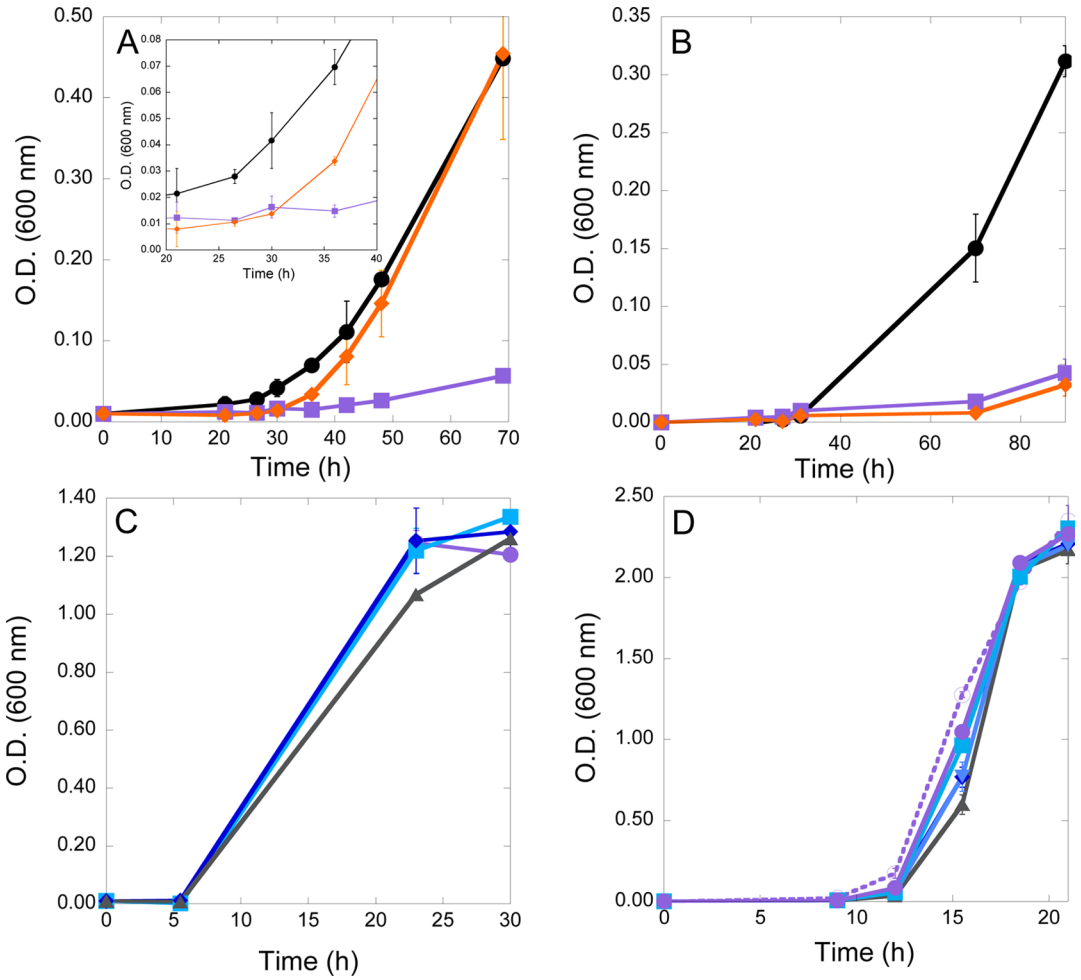

Figure 5. *P. aeruginosa* growth studies with C13-B$(OH)_2$. (A) In iron-limited minimum medium, the growth of wild-type *P. aeruginosa* in the absence of inhibitor (black ●) or after initial treatment with 1 μM inhibitor (orange ◆) is shown in comparison to the untreated tranposon *pvdQ* insertion mutant *P. aeruginosa* strain (purple ■). O.D. is optical density. Inset shows 20–40 h in more detail. (B) Same experiment as in panel A, except all incubations also contain 40 μM PAβN. (C) In minimal media containing trace iron, the growth of the transposon *pvdQ* insertion mutant *P. aeruginosa* strain is shown in the presence of 0 (purple ●), 0.1 (light blue ■), 10 (dark blue ◆), and 100 (gray ▲) μM inhibitor. (D) Same experiment as in panel C, with an additional concentration of inhibitor (1 μM,), except each incubation also contains 40 μM PAβN, and one incubation (purple ○, dashed line) contains neither inhibitor nor PAβN.

and Arg513 (3.5 Å). The *N*-terminal amine can again act directly as a general acid to protonate the leaving group and as a general base to generate a hydroxide ion required to attack the ester intermediate (path 3a). In contrast to amides, PNP esters

dx.doi.org/10.1021/cb400345h | *ACS Chem. Biol.* 2013, 8, 2192–2200

have leaving groups that do not require protonation and would therefore not supply the general base needed to generate hydroxide in path 3b. Yet, the PNP esters described here are excellent substrates, and so favor a product-independent pathway for intermediate decay (path 3a). Attack of hydroxide ion leads to formation of the second tetrahedral adduct (Figure 4, boxed). The C13-B$(OH)_2$−PvdQ complex most closely resembles this catalytic intermediate and provides some insight into its formation and stabilization. Based on comparison of the transition-state analogue to a trapped ester intermediate,[18,28] the incoming hydroxide ion in step 4 appears to attack the *re* face of the ester. As proposed earlier,[28] an "oxyanion" hole, consisting of the backbone nitrogen of Val268 and the side chain nitrogen of Asn485, provides H-bonds to one of the oxygens in the tetrahedral adduct. Additionally, the oxygen corresponding to the incoming nucleophilic hydroxide is stabilized by H-bonds to both the backbone nitrogen and carbonyl of His239 and is also close (2.7 Å) to the *N*-terminus of Ser217. Collapse of the tetrahedral adduct leads to C−O bond cleavage and protonation of the Ser217 side chain. The C13-B$(OH)_2$−PvdQ complex shows a 2.8 Å distance from this oxygen to the *N*-terminal amine, supporting a direct proton transfer (path 5a) rather than transfer through an intervening water (path 5b). The closest ordered water molecule observed is 5.8 Å distant and overlaps with the position likely occupied by the leaving group amine in the first tetrahedral intermediate, disfavoring paths 3b and 5b. The fatty acid product (P_2) can then dissociate to regenerate resting enzyme (path 6).

Cultured Cell Growth Assays. Previously, different enzymes in siderophore biosynthesis have been effectively targeted by inhibitor design and high-throughput screening. Inhibitors of aryl acid adenylating enzymes potently inhibit siderophore production and/or iron-limited growth of *M. tuberculosis*, *Y. pestis*, and other microorganisms.[8−10] These compounds might also have potential applications with *P. aeruginosa* due to similarities of their target enzymes with the adenylating enzyme PchD used in pyochelin production. To the best of our knowledge, only one report describes a siderophore biosynthetic inhibitor that was applied to *P. aeruginosa* growth. Micromolar concentrations of the PvdQ inhibitor ML318 inhibits growth of *P. aeruginosa* in iron-limiting conditions.[11] Here, we extend the study of iron-limited *P. aeruginosa* growth to alkylboronate inhibitors of PvdQ.

The PvdQ inhibitor C13-B$(OH)_2$ was tested for its effects in cell culture (Figure 5). Wild-type *P. aeruginosa* can grow in iron-limited minimal media, but the transposon-disrupted *pvdQ* mutant strain shows only very limited growth. Wild-type *P. aeruginosa* cultures given an initial dose of 1 μM inhibitor (5000 × K_i) are growth inhibited. However, after 30 h, growth of the inhibitor-treated culture recovers and then parallels that of the untreated wild-type strain (Figure 5A). Recovery cannot be avoided by repeated dosing of the inhibitor (not shown).

These experiments were then repeated in the presence of phenylalainine-arginine-β-naphthylamide (PAβN; CAS 100929-99-5), a wide-spectrum competitive inhibitor of multidrug-resistance efflux pumps that can also increase outer membrane permeability through other mechanisms.[30] Co-administration of both C13-B$(OH)_2$ and PAβN severely inhibits growth of wild-type *P. aeruginosa* under iron-limited conditions, and growth does not recover like it did in the absence of PAβN (Figure 5B). These studies indicate that the PvdQ inhibitor C13-B$(OH)_2$ can inhibit the growth of *P. aeruginosa* in iron-limited conditions, but that the efficacy of this particular compound in cell culture is likely limited by poor access to the target due to outer membrane impermeability or a multidrug efflux pump. It has been reported that compounds structurally similar to C13-B$(OH)_2$, including *N*-acyl-HSLs and sodium dodecyl sulfate, are exported by the MexAB-OprM efflux pump, but other efflux pumps might also play a role.[31,32]

As predicted, when iron is not limiting, control experiments using the same concentrations of inhibitors to treat the transposon-disrupted *pvdQ* strain do not result in a similar growth inhibition (Figure 5C and D). This result is consistent with our proposal that C13-B$(OH)_2$ targets iron acquisition. Higher concentrations of C13-B$(OH)_2$ do result in minor growth inhibition (Figure 5C), which suggests that this particular inhibitor may have deleterious off-target effects when used at elevated concentrations. This result is not entirely unexpected due to the hydrophobicity and structural simplicity of the unsubstituted n-alkyl substituent. However, to the best of our knowledge, this is the first rationally designed boron-containing inhibitor of siderophore biosynthesis shown to block the growth of *P. aeruginosa* in iron-limited conditions and serves as a proof of principle.

In summary, PvdQ is revealed to have high specificity constants for myristoylated substrates, yet it discriminates against *N*-acyl-HSLs produced endogenously by *P. aeruginosa*. This finding supports the conclusion that PvdQ has not primarily evolved to regulate quorum-sensing endogenous to *P. aeruginosa*. However, the quorum-quenching ability of PvdQ remains useful as a biochemical tool to target a narrow set of quorum-sensing signals. To counteract the primary role of PvdQ in siderophore production, we identified *n*-alkylboronic acids as extremely potent PvdQ inhibitors, due in part to the similarity of their monocovalent tetrahedral adducts to the reaction transition state. One of the most potent compounds, 1-tridecylboronic acid (C13-B$(OH)_2$), inhibits growth of *P. aeruginosa* in iron-limited media and serves as a proof of principle. The efficacy of this particular compound is limited by poor target access and likely by limited selectivity due to its unsubstituted alkyl moiety. However, since boron-based inhibitors are used clinically[20] and have proven useful in cultured *P. aeruginosa*,[33] we suggest that this moiety may be a productive chemotype to retain in the design of more biologically effective PvdQ inhibitors.

METHODS

Materials. Unless otherwise noted, all chemicals were obtained from Sigma-Aldrich Chemical Co. (St. Louis, MO, USA), and all restriction enzymes were from New England BioLabs (Beverly, MA, USA). 1-Octylboronic acid (C8-B$(OH)_2$), 1-decylboronic acid (C10-B$(OH)_2$), 1-dodecylboronic acid (C12-B$(OH)_2$), and 1-tetradecylboronic acid (C14-B$(OH)_2$) were from Alfa Aesar (Ward Hill, MA, USA). *p*-Nitrophenyl esters of capric (C10-PNP), lauric (C12-PNP), myristic (C14-PNP), and palmitic (C16-PNP) acids were from Research Organics, Cleveland, OH. Syringe filters are MillexGP filter units (0.22 μm, PES membrane, Millipore). PAβN was from Bachem (Torrance, California).

3-Oxo-dodecanoyl-homoserine lactone (3-oxo-C12-HSL) is known to undergo non-enzymatic rearrangement.[34] To verify the stock solutions of this compound had not rearranged from the lactone (which is susceptible to AiiA mediated hydrolysis) to the tetramic acid (which is not), LC-ESI-MS (+ ionization) was used to show an 18 Da increase between untreated (298.2 Da) and AiiA^{35}-treated (316.2) samples, consistent with maintaining an intact lactone, 3-oxo-C12-HSL, in the stock solution.

1-Tridecylboronic acid (C13-B$(OH)_2$) was synthesized in two steps using a published route for butylboronic acid,[36] but substituting

tridecylic acid for butyric acid. The product was recrystallized from hexanes as white needles (57% yield). ^{1}H NMR (DMSO): δ 7.28 (s, 2H), 1.26 (m, 22H), 0.84 (t, J = 6.5 Hz, 3H), 0.55 (t, J = 7.5 Hz, 2H). ^{13}C NMR (DMSO): δ 32.1, 31.3, 29.1, 29.0, 28.7, 24.2, 22.1, 15.4, 13.9. ^{11}B NMR (DMSO): δ 32.4. HRMS: $[M - H]^-$ calcd for $C_{13}H_{28}BO_2$ 227.2190, found 227.2190.

Cloning, Expression, and Purification. *P. aeruignosa* PvdQ was obtained by heterologous expression from *E. coli* using standard methodology described in Supporting Information.

Activity and Inhibition Assays. Steady-state kinetic constants were determined for hydrolysis of two substrate classes. PNP-ester hydrolysis[18] was continuously monitored using UV−vis absorbance spectroscopy (Varian Cary 50) to detect formation of *p*-nitrophenolate; ε_{402nm} = 13,000 M^{-1} cm^{-1}. The ε_{402nm} was determined experimentally using the assay buffer. Substrate stock solutions were prepared in methanol, which was determined to be an acceptable assay cosolvent (Supplementary Figure S5). Assays were completed using disposable polystyrene cuvettes (Thermo Fisher), substrate, Na_2HPO_4 (40 mM) at pH 8.0, 25 °C with 20% methanol as a cosolvent and were initiated with addition of PvdQ (10 nM). Fresh working dilutions of PvdQ (1 μM) were made from more concentrated stocks after each hour of use. Assay buffer was filtered prior to use to eliminate dust particles. Initial hydrolysis rates (<10% substrate consumed) were linear. KaleidaGraph 3.6 (Synergy Software, Reading, PA, USA) was used to determine k_{cat} and K_M values and associated error by nonlinear fitting to the Michaelis−Menten equation. Values determined here are signifigantly different than previous reported values (e.g., C12-PNP, K_M = 1.4 mM, k_{cat} 44 min^{-1}).[18] In our hands, the substrates were not sufficiently soluble to use the previously reported assay conditions. Here, inclusion of well-tolerated cosolvent (Supplemetary Figure S5) led to improved kinetic parameters (e.g., C12-PNP, K_M = 0.6 μM, k_{cat} 86 min^{-1}) (Table 1).

N-Acyl-HSL amide hydrolysis was monitored with an end point assay by *o*-phthaldialdehyde (OPA) derivitization of the product amine [37] followed by HPLC and fluorescence detection compared to a standard curve prepared each day using (*S*)-(−)-α-amino-γ-butyrolactone (linear from 30 nM to 100 μM). Assay details are supplied in Supporting Information.

Initial screening for PvdQ inhibition by fatty acids and boronic acids was accomplished using a method similar to the PNP-ester assay described above except using a Wallac Victor^2 plate reader (PerkinElmer, Waltham MA), one concentration of C12-PNP (5 μM) and varying concentrations of fatty acids and boronic acids, diluted from DMSO stock solutions, in triplicate. Final assays do not exceed 1% DMSO (v/v), which does not inhibit PvdQ.

Concentration−response curves for C10-, C14-, and C15-$B(OH)_2$ were determined in the same fashion and fit to determine IC_{50} values. The IC_{50} for C8-$B(OH)_2$ was also measured this way, but using a Cary 50 spectrophotometer instead of a plate reader. These IC_{50} values were then converted to K_i values for a tight-binding competitive inhibition model described elsewhere[22] using enzyme concentration as determined by A_{280nm} (Supporting Information). Because these compounds have IC_{50} values greater than the enzyme concentration, small variations in enzyme concentration have less of an impact on K_i than with the more potent inhibitors below.

The K_i values and the mode of inhibition for C12- and C13-$B(OH)_2$ were determined using a slightly modified method. Briefly, PvdQ activity was measured in singlicate assays using disposable polystyrene cuvettes and a Cary-50 UV−vis spectrophotometer as above to determine IC_{50} values at different concentrations of C12-PNP. The IC_{50} values were plotted against $[C12\text{-}PNP]/K_M$ values to determine mode of inhibition and K_i values, as described elsewhere (Supplementary Figure S1).[22] Due to the potency of these tight-binding inhibitors, small changes in inhibitor or enzyme concentrations can impact IC_{50} values, so in contrast to the inhibitors above, all kinetic experiments for C12- and C13-$B(OH)_2$ were performed on the same day using the same enzyme and inhibitor stock solutions.

Crystallography. Cocrystals of PvdQ and C13-$B(OH)_2$ were grown by hanging drop vapor diffusion by mixing PvdQ (10 mg mL^{-1}), C13-$B(OH)_2$ (50 mM in DMSO), and crystallization solution (0.05 M Hepes at pH 7.5); 80 mM RbCl; 9% PEG 4000 and 20% glycerol, which is slightly modified from a previously reported condition[18]) at a ratio of 1:0.5:1 μL, respectively, at 20 °C. Crystals appeared in 1 h and grew to maximum size in 5 days. Those with good morphology and typical dimensions of 0.5 mm × 0.3 mm × 0.2 mm were picked and flash cooled in $N_{2(l)}$. X-ray diffraction data sets were collected at the Advanced Photon Source, beamline 23-ID, Argonne National Laboratory. The wavelength used in monochromatic data collection was 1.0332 Å. All collected data sets were indexed and integrated using iMosflm[38] and scaled in program Scala in CCP4.[39] The best data set was processed to a resolution of 1.8 Å.

The PvdQ−C13-$B(OH)_2$ structure was solved by molecular replacement using the program PHASER with a starting model of a reported structure of PvdQ (PDB ID: 2WYE[28]). The structural solution of the protein was obtained, and an extended region of positive difference electron density ($F_o - F_c$ map) was identified (not shown; see Figure 3B for a simulated annealing composite omit map). This observed extra density corresponds to the omitted inhibitor moiety at the active site. Once a structural solution was obtained, model building was conducted in COOT.[40] A structural file of the C13-$B(OH)_2$−Ser217 adduct was created in Chemdraw (Perkin-Elmer, Cambridge, MA, USA); the generated structure of the adduct was used to generate chemical restraints using JLigand.[41] The covalent adduct was fitted into the observed extra electron density using COOT. Rigid body refinement and restrained refinement were conducted using program REFMAC5 in CCP4. Manual adjustments and rebuilding of the structural model were conducted using COOT; further refinements were carried out using PHENIX,[42] including TLS refinement[43] and simulated annealing refinement. Structural figures of the protein were created using UCSF Chimera.[44]

***P. aeruginosa* Growth Assays.** The effect of C13-$B(OH)_2$ on cultured cells was monitored using wild-type *P. aeruginosa* PA14 or a transposon-disrupted *pvdQ* mutant, *P. aeruginosa* PA14 ID27758 from the PA14 mutant library.[45] This mutant strain has been used previously to study phenotypes resulting from loss of PvdQ function.[46] Briefly, a 1 mL culture in LB, started from glycerol stocks, is grown with shaking (220 rpm) for approximately 7 h until A_{600nm} is approximately 0.5. Cells were pelleted (5000 × g), washed three times with sterile phosphate-buffered saline (PBS), and resuspended in 250 μL of sterile iron-limited MOPS glucose medium (25 mM morpholinepropanesulfonic acid at pH 7.2, 93 mM NH_4Cl, 43 mM NaCl, 3.7 mM KH_2PO_4, 1 mM $MgSO_4$, 45 μM diethylene triamine pentaacetic acid (DTPA), 20 mM glucose).[47] DTPA was added to chelate any trace iron, as described elsewhere.[48] Triplicate cultures (1 mL) in the same medium were then inoculated to a starting OD_{600} of 0.01, treated with either vehicle alone (DMSO, 0.1% v/v) or C13-$B(OH)_2$ (1 μM), and incubated with shaking at 37 °C for up to 70 h. Tests for off-target toxicity were completed in the same manner using the *pvdQ* mutant *P. aeruginosa* strain and the same culture medium, but omitting DTPA and instead supplementing with $FeSO_4$ (3.5 μM)[47] and treating with various inhibitor concentrations (1 nM to 100 μM). When indicated, stock solutions of PAβN (200 mM in DMSO) were diluted into cultures to a final concentration of 40 μM.

■ ASSOCIATED CONTENT

Supporting Information

This material is available free of charge via the Internet at http://pubs.acs.org.

Accession Codes

Coordinates of the PvdQ−C13-$B(OH)_2$ complex have been deposited in the Protein Data Bank with the accession number 4M1J.

■ AUTHOR INFORMATION

Corresponding Author

*E- mail: walt.fast@austin.utexas.edu; dliu@luc.edu.

Notes

The authors declare no competing financial interest.

■ ACKNOWLEDGMENTS

We thank the following for generous gifts: M. Whitely (Univ. of Texas, Austin) for *P. aeruginosa* PA14 ID27758, J. Leadbetter (CA Inst Tech) for a PvdQ expression plasmid, and W. Bachovchin & D. O'Connell (Tufts University) for 1-pentadecylboronic acid (C15-B(OH)$_2$). We thank J. Golihar (Univ. of Texas, Austin) for help designing the growth assays. This work was supported in part by the Robert A. Welch Foundation (Grant F-1572 to W.F.) and by Loyola University Chicago (to D.L.). We thank Ruslan Sanishvili (GM/CA-CAT, sector 23) at Advanced Photon Source, Argonne National Laboratory (Argonne, IL) for help with data collection; GM/CA at APS has been funded in whole or in part with Federal funds from the National Cancer Institute (Y1-CO-1020) and the National Institute of General Medical Sciences (Y1-GM-1104). Use of the Advanced Photon Source was supported by the U.S. Department of Energy, Basic Energy Sciences, Office of Science, under contract No. DE-AC02-06CH11357.

■ REFERENCES

(1) Navon-Venezia, S., Ben-Ami, R., and Carmeli, Y. (2005) Update on *Pseudomonas aeruginosa* and *Acinetobacter baumannii* infections in the healthcare setting. *Curr. Opin. Infect. Dis. 18*, 306−313.

(2) Frederick, R. E., Mayfield, J. A., and DuBois, J. L. (2009) Iron trafficking as an antimicrobial target. *Biometals 22*, 583−593.

(3) Romero, M., Acuna, L., and Otero, A. (2012) Patents on quorum quenching: interfering with bacterial communication as a strategy to fight infections. *Recent Pat. Biotechnol. 6*, 2−12.

(4) Huang, J. J., Han, J. I., Zhang, L. H., and Leadbetter, J. R. (2003) Utilization of acyl-homoserine lactone quorum signals for growth by a soil pseudomonad and *Pseudomonas aeruginosa* PAO1. *Appl. Environ. Microbiol. 69*, 5941−5949.

(5) Hannauer, M., Schafer, M., Hoegy, F., Gizzi, P., Wehrung, P., Mislin, G. L., Budzikiewicz, H., and Schalk, I. J. (2012) Biosynthesis of the pyoverdine siderophore of *Pseudomonas aeruginosa* involves precursors with a myristic or a myristoleic acid chain. *FEBS Lett. 586*, 96−101.

(6) Otto, B. R., Verweij-van Vught, A. M., and MacLaren, D. M. (1992) Transferrins and heme-compounds as iron sources for pathogenic bacteria. *Crit. Rev. Microbiol. 18*, 217−233.

(7) Schalk, I. J., and Guillon, L. (2012) Pyoverdine biosynthesis and secretion in *Pseudomonas aeruginosa*: implications for metal homeostasis. *Environ. Microbiol. 15*, 1661−1673.

(8) Ferreras, J. A., Ryu, J. S., Di Lello, F., Tan, D. S., and Quadri, L. E. (2005) Small-molecule inhibition of siderophore biosynthesis in *Mycobacterium tuberculosis* and *Yersinia pestis*. *Nat. Chem. Biol. 1*, 29−32.

(9) Neres, J., Wilson, D. J., Celia, L., Beck, B. J., and Aldrich, C. C. (2008) Aryl acid adenylating enzymes involved in siderophore biosynthesis: fluorescence polarization assay, ligand specificity, and discovery of non-nucleoside inhibitors via high-throughput screening. *Biochemistry 47*, 11735−11749.

(10) Somu, R. V., Boshoff, H., Qiao, C., Bennett, E. M., Barry, C. E., 3rd, and Aldrich, C. C. (2006) Rationally designed nucleoside antibiotics that inhibit siderophore biosynthesis of *Mycobacterium tuberculosis*. *J. Med. Chem. 49*, 31−34.

(11) Theriault, J. R., Wurst, J., Jewett, I., Verplank, L., Perez, J. R., Gulick, A. M., Drake, E. J., Palmer, M., Moskowitz, S., Dasgupta, N., Brannon, M. K., Dandapani, S., Munoz, B., and Schreiber, S. (2013) Identification of a small molecule inhibitor of *Pseudomonas aeruginosa* PvdQ acylase, an enzyme involved in siderophore pyoverdine synthesis, *Probe Reports from NIH Molecular Libraries Program*, National Center for Biotechnology Information, Bethesda, MD.

(12) Nadal Jimenez, P., Koch, G., Papaioannou, E., Wahjudi, M., Krzeslak, J., Coenye, T., Cool, R. H., and Quax, W. J. (2010) Role of PvdQ in *Pseudomonas aeruginosa* virulence under iron-limiting conditions. *Microbiology 156*, 49−59.

(13) Sio, C. F., Otten, L. G., Cool, R. H., Diggle, S. P., Braun, P. G., Bos, R., Daykin, M., Camara, M., Williams, P., and Quax, W. J. (2006) Quorum quenching by an N-acyl-homoserine lactone acylase from *Pseudomonas aeruginosa* PAO1. *Infect. Immun. 74*, 1673−1682.

(14) Wahjudi, M., Murugappan, S., van Merkerk, R., Eissens, A. C., Visser, M. R., Hinrichs, W. L., and Quax, W. J. (2012) Development of a dry, stable and inhalable acyl-homoserine-lactone-acylase powder formulation for the treatment of pulmonary *Pseudomonas aeruginosa* infections. *Eur. J. Pharm. Sci. 48*, 637−643.

(15) Thomas, P. W., Stone, E. M., Costello, A. L., Tierney, D. L., and Fast, W. (2005) The quorum-quenching lactonase from *Bacillus thuringiensis* is a metalloprotein. *Biochemistry 44*, 7559−7569.

(16) Chow, J. Y., Wu, L., and Yew, W. S. (2009) Directed evolution of a quorum-quenching lactonase from *Mycobacterium avium* subsp. paratuberculosis K-10 in the amidohydrolase superfamily. *Biochemistry 48*, 4344−4353.

(17) Momb, J., Wang, C., Liu, D., Thomas, P. W., Petsko, G. A., Guo, H., Ringe, D., and Fast, W. (2008) Mechanism of the quorum-quenching lactonase (AiiA) from *Bacillus thuringiensis*. 2. Substrate modeling and active site mutations. *Biochemistry 47*, 7715−7725.

(18) Drake, E. J., and Gulick, A. M. (2011) Structural characterization and high-throughput screening of inhibitors of PvdQ, an NTN hydrolase involved in pyoverdine synthesis. *ACS Chem. Biol. 6*, 1277−1286.

(19) Copley, S. D. (2012) Moonlighting is mainstream: paradigm adjustment required. *Bioessays 34*, 578−588.

(20) Baker, S. J., Ding, C. Z., Akama, T., Zhang, Y. K., Hernandez, V., and Xia, Y. (2009) Therapeutic potential of boron-containing compounds. *Future Med. Chem. 1*, 1275−1288.

(21) Smoum, R., Rubinstein, A., Dembitsky, V. M., and Srebnik, M. (2012) Boron containing compounds as protease inhibitors. *Chem. Rev. 112*, 4156−4220.

(22) Copeland, R. A. (2005) *Evaluation of Enzyme Inhibitors in Drug Discovery: A Guide for Medicinal Chemists and Pharmacologists*, pp 178−213, Wiley-Interscience, Hoboken, NJ.

(23) Philipp, M., and Bender, M. L. (1971) Inhibition of serine proteases by arylboronic acids. *Proc. Natl. Acad. Sci. U.S.A. 68*, 478−480.

(24) Zervosen, A., Herman, R., Kerff, F., Herman, A., Bouillez, A., Prati, F., Pratt, R. F., Frere, J. M., Joris, B., Luxen, A., Charlier, P., and Sauvage, E. (2011) Unexpected tricovalent binding mode of boronic acids within the active site of a penicillin-binding protein. *J. Am. Chem. Soc. 133*, 10839−10848.

(25) Transue, T. R., Krahn, J. M., Gabel, S. A., DeRose, E. F., and London, R. E. (2004) X-ray and NMR characterization of covalent complexes of trypsin, borate, and alcohols. *Biochemistry 43*, 2829−2839.

(26) Katz, B. A., Finer-Moore, J., Mortezaei, R., Rich, D. H., and Stroud, R. M. (1995) Episelection: novel Ki ∼ nanomolar inhibitors of serine proteases selected by binding or chemistry on an enzyme surface. *Biochemistry 34*, 8264−8280.

(27) Bachovchin, W. W., Wong, W. Y., Farr-Jones, S., Shenvi, A. B., and Kettner, C. A. (1988) Nitrogen-15 NMR spectroscopy of the catalytic-triad histidine of a serine protease in peptide boronic acid inhibitor complexes. *Biochemistry 27*, 7689−7697.

(28) Bokhove, M., Nadal Jimenez, P., Quax, W. J., and Dijkstra, B. W. (2010) The quorum-quenching N-acyl homoserine lactone acylase PvdQ is an Ntn-hydrolase with an unusual substrate-binding pocket. *Proc. Natl. Acad. Sci. U.S.A. 107*, 686−691.

(29) Chilov, G. G., Sidorova, A. V., and Svedas, V. K. (2007) Quantum chemical studies of the catalytic mechanism of N-terminal nucleophile hydrolase. *Biochemistry (Mosc) 72*, 495−500.

(30) Lomovskaya, O., Warren, M. S., Lee, A., Galazzo, J., Fronko, R., Lee, M., Blais, J., Cho, D., Chamberland, S., Renau, T., Leger, R., Hecker, S., Watkins, W., Hoshino, K., Ishida, H., and Lee, V. J. (2001) Identification and characterization of inhibitors of multidrug resistance efflux pumps in *Pseudomonas aeruginosa*: novel agents for combination therapy. *Antimicrob. Agents Chemother. 45*, 105−116.

(31) Pearson, J. P., Van Delden, C., and Iglewski, B. H. (1999) Active efflux and diffusion are involved in transport of *Pseudomonas aeruginosa* cell-to-cell signals. *J. Bacteriol. 181*, 1203−1210.
(32) Srikumar, R., Kon, T., Gotoh, N., and Poole, K. (1998) Expression of *Pseudomonas aeruginosa* multidrug efflux pumps MexA-MexB-OprM and MexC-MexD-OprJ in a multidrug-sensitive *Escherichia coli* strain. *Antimicrob. Agents Chemother. 42*, 65−71.
(33) Hernandez, V., Crepin, T., Palencia, A., Cusack, S., Akama, T., Baker, S. J., Bu, W., Feng, L., Freund, Y. R., Liu, L., Meewan, M., Mohan, M., Mao, W., Rock, F. L., Sexton, H., Sheoran, A., Zhang, Y., Zhang, Y. K., Zhou, Y., Nieman, J. A., Anugula, M. R., Keramane el, M., Savariraj, K., Reddy, D. S., Sharma, R., Subedi, R., Singh, R., O'Leary, A., Simon, N. L., De Marsh, P. L., Mushtaq, S., Warner, M., Livermore, D. M., Alley, M. R., and Plattner, J. J. (2013) Discovery of a novel class of boron-based antibacterials with activity against gram-negative bacteria. *Antimicrob. Agents Chemother. 57*, 1394−1403.
(34) Kaufmann, G. F., Sartorio, R., Lee, S. H., Rogers, C. J., Meijler, M. M., Moss, J. A., Clapham, B., Brogan, A. P., Dickerson, T. J., and Janda, K. D. (2005) Revisiting quorum sensing: Discovery of additional chemical and biological functions for 3-oxo-N-acylhomoserine lactones. *Proc. Natl. Acad. Sci. U.S.A. 102*, 309−314.
(35) Thomas, P. W., and Fast, W. (2011) Heterologous overexpression, purification, and in vitro characterization of AHL lactonases. *Methods Mol. Biol. 692*, 275−290.
(36) Charette, A. B., and Lebel, H. (1999) (2*S*,3*S*)-(+)-(3-Phenylcyclopropyl)methanol. *Org. Synth. 76*, 86.
(37) Xu, F., Byun, T., Deussen, H. J., and Duke, K. R. (2003) Degradation of N-acylhomoserine lactones, the bacterial quorum-sensing molecules, by acylase. *J. Biotechnol. 101*, 89−96.
(38) Battye, T. G., Kontogiannis, L., Johnson, O., Powell, H. R., and AG, L. (2011) iMOSFLM: a new graphical interface for diffraction-image processing with MOSFLM. *Acta Crystallogr., Sect. D: Biol. Crystallogr. 67*, 27−81.
(39) Collaborative Computation Project (1994) The CCP4 suite: programs for protein crystallography. *Acta Crystallogr., Sect. D: Biol. Cyrstallogr. 50*, 760−763.
(40) Emsley, P., and Cowtan, K. (2004) Coot: model-building tools for molecular graphics. *Acta Crystallogr., Sect. D: Biol. Crystallogr. 60*, 2126−2132.
(41) Lebedev, A. A., Young, P., Isupov, M. N., Moroz, O. V., Vagin, A. A., and Murshudov, G. N. (2012) JLigand: a graphical tool for the CCP4 template-restraint library. *Acta Crystallogr., Sect. D: Biol. Crystallogr. 68*, 431−440.
(42) Adams, P. D., Grosse-Kunstleve, R. W., Hung, L.-W., Ioerger, T. R., McCoy, A. J., Moriarty, N. W., Read, R. J., Sacchettini, J. C., Sauter, N. K., and Terwilliger, T. C. (2002) PHENIX: building new software for automated crystallographic structure determination. *Acta Crystallogr., Sect. D: Biol. Crystallogr. 58*, 1948−1954.
(43) Winn, M. D., Isupov, M. N., and Murshudov, G. N. (2001) Use of TLS parameters to model anisotropic displacements in marcromolecular refinement. *Acta Crystallogr., Sect. D: Biol. Crystallogr. 57*, 122−133.
(44) Pettersen, E. F., Goddard, T. D., Huang, C. C., Couch, G. S., Greenblatt, D. M., Meng, E. C., and Ferrin, T. E. (2004) UCSF Chimera–a visualization system for exploratory research and analysis. *J. Comput. Chem. 25*, 1605−1612.
(45) Liberati, N. T., Urbach, J. M., Miyata, S., Lee, D. G., Drenkard, E., Wu, G., Villanueva, J., Wei, T., and Ausubel, F. M. (2006) An ordered, nonredundant library of *Pseudomonas aeruginosa* strain PA14 transposon insertion mutants. *Proc. Natl. Acad. Sci. U.S.A. 103*, 2833−2838.
(46) Overhage, J., Bains, M., Brazas, M. D., and Hancock, R. E. (2008) Swarming of *Pseudomonas aeruginosa* is a complex adaptation leading to increased production of virulence factors and antibiotic resistance. *J. Bacteriol. 190*, 2671−2679.
(47) Korgaonkar, A. K., and Whiteley, M. (2011) *Pseudomonas aeruginosa* enhances production of an antimicrobial in response to N-acetylglucosamine and peptidoglycan. *J. Bacteriol. 193*, 909−917.
(48) Fung, C., Naughton, S., Turnbull, L., Tingpej, P., Rose, B., Arthur, J., Hu, H., Harmer, C., Harbour, C., Hassett, D. J., Whitchurch, C. B., and Manos, J. (2010) Gene expression of Pseudomonas aeruginosa in a mucin-containing synthetic growth medium mimicking cystic fibrosis lung sputum. *J. Med. Microbiol. 59*, 1089−1100.